RSC Advances

PAPER

View Article Online
View Journal | View Issue

Cite this: *RSC Adv.*, 2017, **7**, 55920

MOF derived mesoporous K-ZrO_2 with enhanced basic catalytic performance for Knoevenagel condensations†

Peng Wang,*[ab] Jian Feng,[ab] Yupei Zhao,[ab] Sai Gu[c] and Jian Liu *[cd]

Received 13th November 2017
Accepted 5th December 2017

DOI: 10.1039/c7ra12378g

rsc.li/rsc-advances

Mesoporous K-ZrO_2 are designed and synthesized through a direct heat-treatment process of a KNO_3 loaded UiO-66 metal organic framework. Very interestingly, the carbon intermediates formed during the heat-treatment process can act both as mesoporous templates and base-resistant reinforcement for zirconia. The resultant mesoporous K-ZrO_2 catalysts with high surface area show excellent catalytic performance in Knoevenagel condensations, especially for substrates with large molecular size. The mesoporous KZ also show enhanced activity when compared to KZ synthesized from traditional zirconium hydroxides. To the best of our knowledge, this is the first synthesis of a metal-oxide type solid base with a MOF precursor.

Introduction

Acid and base catalysis are very promising for industrial catalytic processes.[1–3] Base catalyzed reactions, such as double bond isomerization, Aldol addition and the Tishchenko reaction, play an important role in production of value-added fine chemicals.[4,5] In industrial practice, the amount of base is nearly stoichiometric, the neutralization of the reaction medium normally produces large amounts of chemical waste. Considering the environmental issues, it is required to substitute the liquid bases and organometallics by solid base catalysts for sustainable and green chemical processes.[6] These solid bases can be varied from metal oxides of mono-component, microporous or mesoporous metal oxides (including silica) immobilized with alkali metals and/or alkali earth metal components, as well as multicomponent metal oxides and salts. Among various solid base catalysts, alkali metal-doped zirconia is very attractive due to its high melting point, low thermal conductivity, and high corrosion resistance.[7] Meanwhile, the incorporation of alkaline metal ions (especially potassium) can generate strong basicity on the surface of zirconia. Traditional synthesis of alkali metal/ZrO_2 consists of immobilization of base precursors on zirconia (*e.g.* alkali metal nitrate, KNO_3) and succedent heat-treatment to convert base precursors to their corresponding metal oxides (*e.g.* K_2O).[8] Considering that zirconia derived from precipitation method usually possess low surface areas, new efforts have been focused on the immobilization of K^+/ZrO_2 (KZ) on mesoporous silica and inducing mesopores into zirconia with the aid of block copolymers as porogens.[9,10] Well-dispersed basic catalytic sites can be produced with enhanced surface areas, which improve the diffusion rate of reactants and products, as well as catalytic performance of the solid base. However, it remains a challenge to design and fabricate mesoporous KZ with high porosity and surface area, while holding the strong basic species on zirconia's external surface.

In the past five years, extensive attention has been paid to metal–organic frameworks (MOFs) derived nanostructures through a thermal decomposition process.[11,12] Due to their porosity and long-range ordering, precise location of catalytic active sites, MOFs exhibit unique advantages over other precursors in the field of solid-state synthesis of porous metal oxides, while highly porous MOFs are an ideal host matrix for loading with active guest components.[13,14] The MOF derived metal oxides can show enhanced catalytic performance compared to traditional precipitated metal-oxides, due to their higher surface areas and more exposed active sites.[15] Therefore, it would be interesting and worthwhile to explore the possibility to synthesize mesoporous KZ from potassium loaded zirconium based MOFs (*e.g.* UiO-66) by using similar strategy. In the light of previous reports, KNO_3 has been chosen as potassium precursor which can generate strong basic sites on zirconia surface during the decomposition of KNO_3 under heat treatment. The aqueous solution of KNO_3 is neutral with the pH value at 7.0, and the well-ordered structures of UiO-66 can be

[a]*Jiangsu Key Laboratory of Advanced Catalytic Materials and Technology, School of Petrochemical Engineering, Changzhou University, Gehu Road 1, Changzhou, Jiangsu 213164, People's Republic of China. E-mail: pengwang@cczu.edu.cn*

[b]*Advanced Catalysis and Green Manufacturing Collaborative Innovation Center, Changzhou University, Gehu Road 1, Changzhou, Jiangsu 213164, People's Republic of China*

[c]*Department of Chemical and Process Engineering, University of Surrey, Guildford, Surrey, GU2 7XH, UK. E-mail: jian.liu@surrey.ac.uk*

[d]*State Key Laboratory of Catalysis, iChEM, Dalian Institute of Chemical Physics, Chinese Academy of Sciences, 457 Zhongshan Road, Dalian 116023, China*

† Electronic supplementary information (ESI) available. See DOI: 10.1039/c7ra12378g

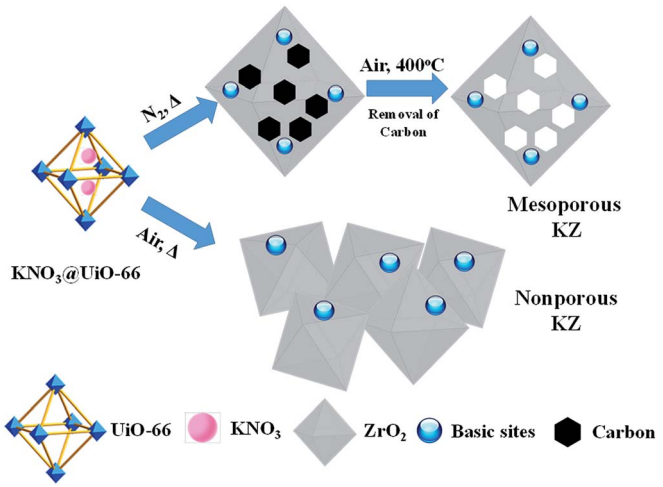

Scheme 1 Illustrations for synthesis of mesoporous KZ from KNO_3-loaded UiO-66 with the two-step heat treatment.

kept in the immersion process for loading KNO_3 into the inner pores of UiO-66. However, a possible predicament in synthesis of KZ with mesopores is the stability of $Zr_6O_4(OH)_4$ nodes of UiO-66 against the corrosion of newborn strongly basic species during calcination.[16] In short, there are more obstacles to be overcome for the synthesis of mesoporous KZ with UiO-66 as precursors, and the reinforcement in stability of ZrO_2's frameworks should be realized to fix the mesopores created during calcination of KNO_3 loaded UiO-66.

Due to the highly ordered crystalline structures, MOFs are proved to be suitable precursors for producing carbon hybrid metal oxides with uniformly distributed components, and the organic ligands in MOFs can be converted into carbon layers which act as the protect shells for metal oxides and provide the possibility to avoid the corrosion of strong base species.[17,18] The homogeneity of carbon distribution is also of great importance as it plays a critical role in stabilization the pore structures of metal oxides, even after removal of the carbon layers with mild calcination. In other words, carbon can act as porous templates for residual metal oxides while the carbon/metal oxides hybrid materials are heated under air with proper procedures. Previous research has proved that carbon can inhibit collapse of the frameworks of iron oxides and produce mesopores for iron-oxides while MOF derived Fe_xO/C hybrids are calcinated under air.[19] Inspiration from this strategy, and considering that carbon are base-resistant materials, a two-step heat-treatment method is adopted to prepare mesoporous KZ from KNO_3 immobilized UiO-66 (Scheme 1, approach A). These KZ materials are characterized with a battery of techniques, and tested in Knoevenagel condensations with substrates of different molecular size.

Experimental

Synthesis of UiO-66

UiO-66 was prepared following a modified procedure as described in literature.[16] In a typical synthetic process, 1.4 g of $ZrCl_4$ and 1.02 g of 1,4-benzenedicarboxylic acid (BDC) were dissolved in 62 mL dimethyl formamide (DMF) and sealed in a stainless-steel vessel with a Teflon liner. The solution was then put into a pre-heated oven at 120 °C. After 24 h, the oven was naturally cooled to room temperature. The activation of UiO-66 was performed by cascade refluxing with DMF and methanol, and the obtained MOF powders were then put in vacuum at 130 °C.

Synthesis of KNO_3@UiO-66

For a typical synthesis, 800 mg UiO-66 suspended in 100 mL of dry *n*-heptane as a hydrophobic solvent and the mixture was sonicated for 15 min until it became homogeneous solution. After stirred of 2 h at 50 °C, 0.8 mL of aqueous potassium nitrate solution of different concentrations as the hydrophilic solvent was added drop-wise over a period of 15 min with constant vigorous stirring. The resulting solution was continuously stirred for 8 h. After careful filtration, the white powder was dried in air at 100 °C. With the adding amounts of 60 mg, 120 mg and 180 mg KNO_3, obtained KNO_3@UiO-66 samples were denoted as UiO-66-1K, UiO-66-2K and UiO-66-3K, respectively, and pure UiO-66 was denoted as UiO-66-0K.

Synthesis of K doped zirconia (KZ) and pure zirconia

For the thermal decomposition process, the as-obtained KNO_3@UiO-66 was calcined firstly at different temperatures in nitrogen for 3 h, followed by heat treatment at 400 °C under air for 6 h. As obtained KZ were denoted as KZ-*x*-*y*-D (*x* and *y* stand for contents of K and the first calcination temperature under N_2 respectively, and two represent the double-step heat treatment). For comparison, KZ prepared with directly calcination under air with single step were denoted as KZ-*x*-*y*-S. For example, UiO-66 loaded with 120 mg KNO_3 resulted in KZ-8.2-650-D while treated at 650 °C under N_2 firstly. Pure zirconia was synthesized by thermal decomposition of UiO-66 under air at 650 °C with one-pot synthesis, and this sample was named as ZrO_2-650-S.

Synthesis of KZ from impregnation of zirconium hydroxide

The catalyst was synthesized by incipient wetness impregnation of an aqueous solution of desired amounts (K contents for *ca.* 8.2 wt%) of potassium nitrate into amorphous zirconium oxy-hydroxide followed by calcination at 650 °C under air for 6 h. The as-obtained catalyst was denoted as KZ-8.2-650-R as reference materials.

Materials characterization

XRD analysis was performed using a Rigaku D/MAX-2500 V/PV diffractometer with Cu-Kα radiation (40 kV and 200 mA) at a scanning speed of 5° min^{-1}. Physisorption of N_2 was performed at −196 °C using a Quantachrome Nova 1200e. Before measurement, the sample was evacuated at 200 °C for 3 h. The surface area was calcinated by the BET method at a relative pressure of $P/P_0 = 0.05$–0.25. Fourier transform infrared (FT-IR) spectra of the samples were collected in transmission mode from KBr pellets at room temperature on a Bruker Tensor 27

spectrometer. Inductively coupled plasma atomic emission spectroscopy (ICP-AES) was carried out to determine the concentration of K in the KZ materials. Prior to the analysis, KZ samples were digested in HF (10 wt%, a.q.) solution with microwave radiation. CO_2 temperature-programmed desorption (CO_2-TPD) experiments were conducted using a Quantachrome ChemBET-3000 analyser. About 200 mg of the sample was pre-treated at 450 °C for 1 h under dry He flow (30 mL min^{-1}), cooled to 50 °C, and then exposed to CO_2 for 0.5 h. After purging the sample with He for 0.5 h, the TPD data were recorded from 50 to 800 °C with a ramping rate of 10 °C min^{-1}.

Catalytic reactions

Knoevenagel condensations of benzaldehyde (BA) and ethylcyanoacetate (ECA)

A 25 mL round-bottom flask was charged with the catalyst (20 mg) in methanol (3 mL), BA (5 mmol) and ECA (6 mmol) while isooctane was used internal standard. The reaction mixture was stirred for 30 min at 35 °C. The solution sample was diluted by ethyl acetate, centrifuged at 10 000 rpm for 2 min, and analyzed by GC (Thermo gas chromatograph equipped with a flame ionization detector and an HP-5 capillary column) to determine the conversion of benzaldehyde, and little by-product (such as benzoic acid) was detected. The catalyst solids were subjected to thermal dehydration at 150 °C for 3 h before their use. Recycled catalysts were washed with ethanol before the next using.

Contrast experiments between KZ-8.2-650-D and KZ-8.2-650-S

500 mg catalysts were immersed in 60 mL methanol with 100 mmol BA or 50 mmol *p*-phenyl benzaldehyde and 120 mmol ECA. The reaction was proceeded at 35 °C and 1 mL samples were taken from the bottle to determine the conversion of BA.

Knoevenagel condensations of BA and diethyl malonate (DEM)

BA (2 mmol) were mixed with 20 mmol DEM with 50 mg catalysts, and the reaction were carried on at 120 °C for 24 h.

Results and discussion

Structural characteristics of solid bases

For a typical synthesis procedure for porous KZ, different concentration of KNO_3 aqueous solutions were injected into heptane-immersed UiO-66 with a double-solvent method, KNO_3 was pumped into inner pores of UiO-66 with the driving force of hydrophilic–hydrophilic interactions.[15] The obtained KNO_3 loaded UiO-66 was firstly treated at different temperatures ranging from 550 to 750 °C under N_2 to decompose KNO_3 and form the carbon-layer protector. The carbon hybrid KZ was further calcinated under air at 400 °C to obtain ultimate product of white KZ-*x*-*y*-D (*y* stands for the first calcination temperature under N_2, and D stands for double times of heat treatments on the samples). It is a remarkable fact that 400 °C is chosen as the temperature to decompose carbon residue, and this temperature is determined on the base of thermogravimetric analysis (TGA) curve of carbon hybrid KZ composite (Fig. S1†). At 400 °C, carbon layers in KZ/C can be eliminated with calcination under air. For comparison, KNO_3@UiO-66 was calcinated directly at different temperatures under air, and the as-synthesized KZ are denoted as KZ-*x*-*y*-S (*x* and *y* represent for the contents of K and calcination temperature respectively, and S represents the single-step heat treatment, Scheme 1, approach B). Pure zirconia was also synthesized by calcination of UiO-66 under air at 650 °C, which is denoted as ZrO_2-650-S.

The porous structures of KZ-*x*-*y* are analyzed with nitrogen sorption techniques. For KZ-*x*-*y*-S, all these samples show typical non-porous adsorption–desorption isotherms with only accumulative pores at high relative pressure (P/P_0 > 0.8, Fig. 1A).[20] In comparison, the sorption isotherms of KZ-*x*-*y*-D exhibit type IV isotherm with a small hysteresis loop in the range between 0.4 and 0.8 for P/P_0, indicating the presence of mesopores (seen in detail, Fig. S2†),[21,22] and accumulative pores between particles of KZ also exist (Fig. 1B). These materials have relatively high BET surface areas between 48 to 84 $m^2\ g^{-1}$ (Table 1), which are almost ten times of surface areas for KZ-*x*-*y*-S series (Table S1†). Such high surface areas are believed to benefit from the two-step calcination of the MOF template. The carbon generated at the first calcination in N_2 can act as a temporal buffer, hindering the further contraction of materials. Moreover, as base-stable materials, carbon layer can protect KZ's frameworks from collapsed by solid basic species which are formed during decomposition of KNO_3 (see below). Nevertheless, KZ-*x*-*y*-S series have very low surface areas (below 10 $m^2\ g^{-1}$ for all samples, Table S1†) as nonporous materials. In addition, pure zirconia (ZrO_2-650-S) has a high BET surface area of 73 $m^2\ g^{-1}$ (Fig. S3†). A possible explanation is that the fragile $Zr_6O_4(OH)_4$ nodes of UiO-66 may be unable to resist the invasion of newborn strongly basic species during calcination and the frameworks of zirconia will collapse to form the nonporous structure of obtained KZ. For UiO-66 without KNO_3, the pore structure has been kept without corrosion of strong basic species.

The evolution of KNO_3 into KZ under heat treatment was also investigated with TG and DSC. Fig. 2 depict TG and DSC curves of UiO-66 loaded with different amounts of KNO_3. Different from UiO-66 which decomposed into carbon hybrid zirconia between 500 and 600 °C, the DSC curves show a much wider peak between the range from 450 to 650 °C which demonstrates

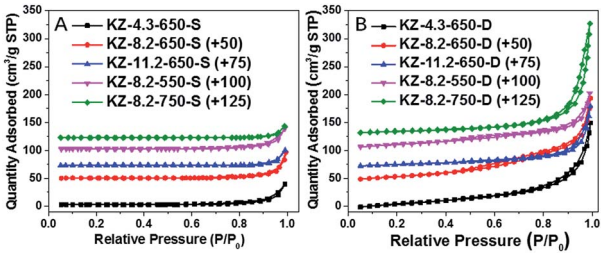

Fig. 1 Nitrogen sorption isotherms of KZ-*x*-*y*-S and KZ-*x*-*y*-D samples (for comparison, the scope of quantity adsorbed are normalized to 350 $cm^3\ g^{-1}$ STP).

Table 1 Porosity, composites and basic properties of KZ prepared under different conditions

Sample	Con. of K[a] (%)	S_{BET}[b] ($m^2\ g^{-1}$)	B_{weak}[c] (mmol g^{-1})	B_{strong}[c] (mmol g^{-1})
KZ-4.3-650-D	4.3	73	0.24	0.09
KZ-8.2-650-D	8.2	80	0.50	0.41
KZ-11.2-650-D	11.2	51	0.44	0.17
KZ-8.2-650-S	8.2[d]	6	0.11	0.07
KZ-8.2-750-D	8.2[d]	49	0.25	0.23
KZ-8.2-550-D	8.2[d]	84	0.42	0.18
KZ-8.2-650-R	8.2[d]	4	0.09	0.08

[a] Contents of K (in weight) are determined with ICP-AES. [b] BET specific surface areas are determined with adsorption data in a relative pressure range of P/P_0 = 0.05–0.25. [c] Base amounts are determined with CO_2-TPD data and 400 °C is chosen as the watershed point to discriminate between weak and strong basic sites. [d] Contents of K are similar to that of KZ-8.2-650-D.

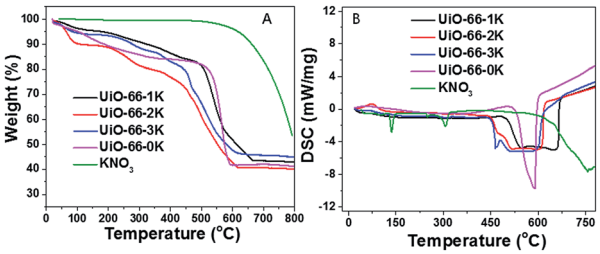

Fig. 2 TG and DSC profiles of UiO-66 loaded with different amounts of KNO_3 and pure KNO_3.

that KNO_3 decomposition have the interaction with decomposition of UiO-66. It proves that high temperature treatment of KNO_3 loaded UiO-66 under N_2 can convert KNO_3 into supported solid base species, as well as transform UiO-66 into carbon hybrid KZ. Furthermore, different from pure KNO_3 with a higher decomposition temperature (>700 °C), UiO-66 improved the decomposition of KNO_3 into supported basic species at moderate temperatures, which is similar with the promotion effect of ZrO_2 as previous reported.[23] The TGA curve of the final KZ-*x*-*y*-D shows no weight loss when heating to 900 °C expect for the desorption of physically adsorbed water around 100 °C (Fig. S4†), and this result proves complete removal of carbon protector at 400 °C under air. Further evidence for elimination of carbon is provided with FT-IR spectra of KZ-*x*-*y*-D (Fig. S5†). The absence of C–H stretching vibrations around 2900 cm^{-1} for KZ-*x*-*y*-D series indicates the almost complete removal of carbon matrix in mesoporous KZ.[24] The XRD patterns of KZ-*x*-*y*-D samples are shown in Fig. 3 to distinguish two crystal phases existing in ZrO_2. Neither characteristic peaks of KNO_3 nor crystallized compound, such as K_2ZrO_3 is detected in these samples. With the increasing contents of K species, the intensity of peaks for the tetragonal form of zirconia raises as the major phase. Only KZ-4.3-650-D with the lowest loading amounts of K species exhibits an obvious mixture of tetragonal (t-ZrO_2) and monoclinic (m-ZrO_2) phase, and it proves that potassium species play a key role in stabling tetragonal phase of zirconia.[25] Due to previous report, K^+ ions are inferred to occupy the position of octa-coordinated Zr^{4+} in t-ZrO_2, which is more stable than the hepta-coordinated Zr^{4+} in m-ZrO_2 because of the interaction of K salt with

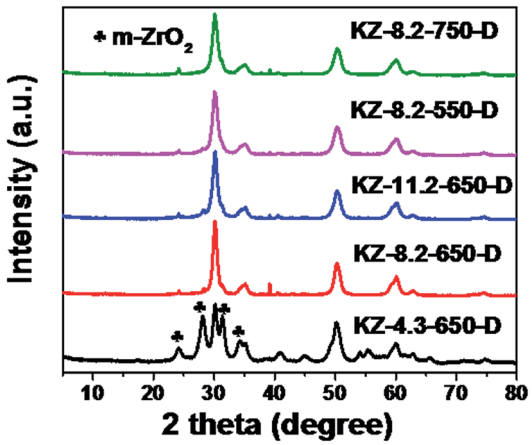

Fig. 3 XRD patterns of KZ-*x*-*y*-D samples (m stands for monoclinic phase of ZrO_2).

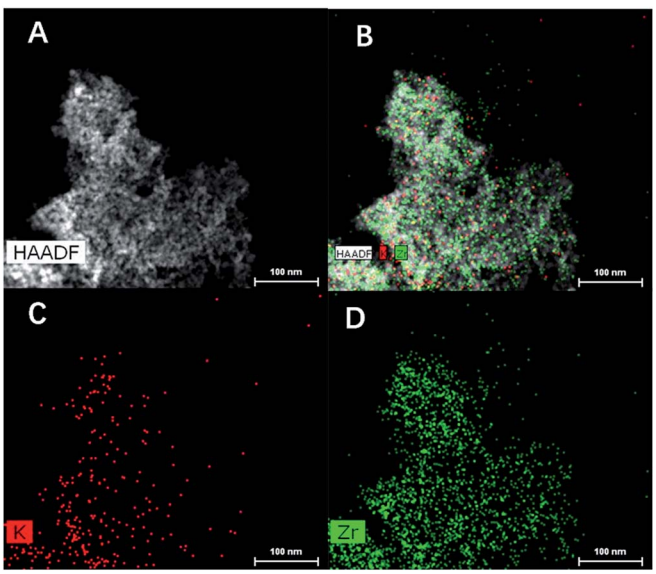

Fig. 4 HAADF (A) and EDX mapping (B) of KZ-8.2-650-D; EDX maps evidencing the macroscopic distribution of (C) K and (D) Zr.

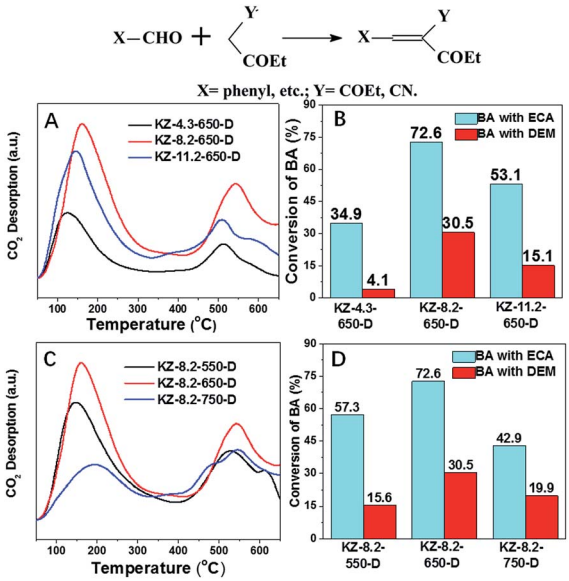

Fig. 5 CO_2-TPD profiles (A, C) and conversions of BA (B, D) with KZ-*x*-*y*-D of different calcination temperature and contents of potassium. Little side product has been produced during the reactions, and the selectivity towards Knoevenagel condensation product is around 95%.

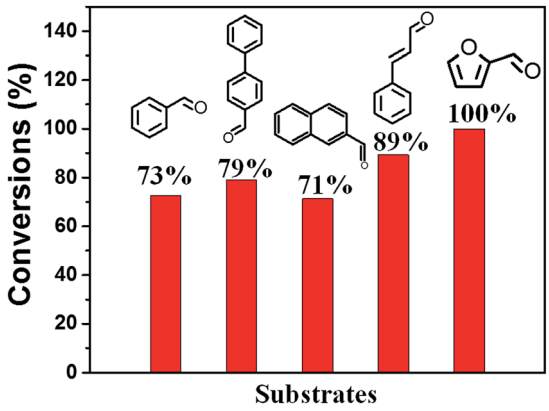

Fig. 6 Catalytic performance of different aldehydes with ethylcyanoacetate over KZ-8.2-650-D. Reaction conditions: aldehyde (5 mmol), ethylcyanoacetate (6 mmol), catalyst (20 mg), methanol (3 mL), 408 K, 30 min. Conversions are determined by GC.

zirconia.[7] Parts of potassium ions incorporate into the lattice of ZrO_2 to stabilize tetragonal crystal form of zirconia. The uniform distribution of potassium on zirconium was further confirmed by energy dispersive X-ray (EDX) spectroscopy with transmission electron microscope (TEM, Fig. 4).

The basic strength and the relative amount of surface basic sites on KZ samples are studied by CO_2-TPD in Fig. 5. There are mainly two kinds of desorption peaks for each mesoporous KZ sample, which indicates that two types of adsorption sites with different basicity coexist on the surface of the solid base.[26] Taking KZ-8.2-650-D as an example, the broad peak between 100 and 300 °C can be ascribed to the weak basic sites of intrinsic zirconia surface as previous report, while the peaks located between 450 and 650 °C are attributed to the strong basic site caused by the introduction of K^+ species to zirconia. It is noticeable that the KZ-8.2-*y*-D series show an intense peak caused by strongly basic sites in addition to weak ones. Moreover, the desorption of CO_2 temperature persists up to 650 °C, which is comparable to some solid superbases, thus revealing the presence of strong basicity on the KZ-8.2-*y*-D samples.[27] According to previous report, the strong basic sites of KZ were attributed to overlapped structure of potassium species on surface of KZ, including K_2O extra-fine particles formed on the composites.[7] The amounts of basic sites due to CO_2-TPD shows a maximum capacity with K contents at 8.2% in weight (Table 1). While increasing loading amounts of K from 8.2% to 11.2%, both amounts of weak and strong basic sites decrease. There are two possible reasons: (1) too much K species can lead to overlapping of basic sites on zirconia's surface and decrease in BET surface areas for KZ as illustrated in table (KZ-11.2-650-D); (2) excessive basic species can also corrode the pore structure of KZ and sequentially bury some K^+ ions in the frameworks of ZrO_2.

On the other hand, there is a similar tendency in CO_2-TPD profiles with different calcination temperature. When treated at 650 °C under N_2, KZ-8.2-650-D (8.2%) shows maximum amounts of both weak and strong basic sites. According to TG profiles of KNO_3 loaded UiO-66, heat treatment at 550 °C can't decompose KNO_3 completely, and KZ-8.2-550-D shows reduced amounts of CO_2-TPD capacity to KZ-8.2-650-D as a result. Further increasing calcination temperature to 750 °C leads to shrinkage of KZ pore structure with the presence of strong base, and it results in decreasing BET surface areas as well as degree of exposure for basic potassium species. On the contrary, nonporous KZ-*x*-*y*-S exhibit much lower amounts of basic sites and this result goes a step further to prove the proportional relationship between BET surface areas and the exposure degree of basic sites. Potassium species play the key role in inducing strong basic sites on the surface of KZ, and there are a few weak basic sites on the surface of pure zirconia, due to the CO_2-TPD profile of ZrO_2-650-S (Fig. S6A†).

Catalytic performance in Knoevenagel condensations

Basic catalytic ability for KZ-*x*-*y*-D series are evaluated in Knoevenagel condensation. Knoevenagel condensations between carbonylic compounds and methylene malonic esters produce several important key products employed in the synthesis of some therapeutic drugs and pharmacological products.[28] Furthermore, catalytic performance of methylene compounds with different acidic character (pK_a) can distinguish status of basic sites with different basic strength. Methylene compounds with higher pK_a values need catalysts of elevated basic strength to deprotonate methylene groups.[29] In this research, ethylcyanoacetate (ECA, $pK_a = 9$) and diethyl malonate (DEM, $pK_a = 13.3$) are tested in condensation with benzaldehyde (BA). Coincide with results of CO_2-TPD (Fig. 5), KZ-8.2-650-D shows highest conversion of BA in reactions with above two methylene substrates. It should be mentioned that KZ-8.2-750-D shows enhanced catalytic performance in condensation of BA and DEM than KZ-8.2-550-D and high temperature treatment

plays a key role in forming enough strong basic sites. On the contrary, KZ-8.2-550-D exhibits better catalytic performance in reactions between BA and ECA, and it is attributed to higher amounts of total basic sites and larger surface areas. Not surprisingly, KZ-4.3-550-D gets the lowest reaction results for both substrates due to its poor basic active sites, and it proves that enough KNO_3 loading amounts in UiO-66 are critical for fabricating strong solid bases. Furthermore, various aldehydes, including furfural and naphthaldehyde were tested in Knoevenagel condensation reactions with ECA as active methylene compounds and KZ-8.2-650-D as catalysts under mild reactions, and all these substrates got good conversions within just 30 min which proved the extensive applicability for KZ-*x*-*y*-D series for Knoevenagel condensations (Fig. 6). Although with high surface area, ZrO_2-650-S resulted in limited catalytic activity (11.2%) in Knoevenagel condensations of BA with ECA under identical reaction conditions (Fig. S6B†), and the selectivity of Knoevenagel condensation product is also poor (47.3%) due to the formation of plenty of benzoic acid by oxidation of BA. The amounts of exposed basic sites, not the surface area, is critical for the catalytic performance.

Further to confirm superiority in pore structures of KZ samples prepared with two-step calcination, contrast experiment between KZ-8.2-650-D and KZ-8.2-650-S is done to evaluate the influence of porosity of KZ on their catalytic performance (Fig. 7), and aldehyde substrates with different sizes are also used to assess the efficiency of mass transfer for KZ samples with different pore structures. Furthermore, KZ-8.2-650-R prepared with traditional zirconium hydroxide as supports is also tested in this reaction as the reference material, and this base catalyst also possesses poor porosity with limited surface areas (Table 1). On both BET surface areas and basic sites' amounts, KZ-8.2-650-D gets much higher scores than its single step treated counterpart and traditional KZ-8.2-650-R. With identical reaction condition, KZ-8.2-650-D with mesoporous

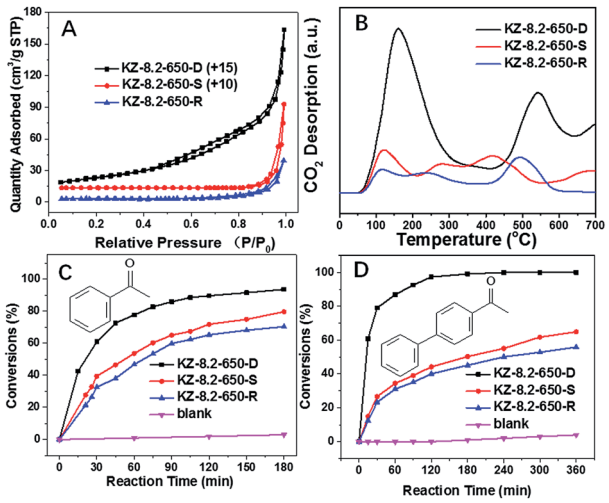

Fig. 7 (A) Nitrogen sorption isotherms, (B) CO_2-TPD profiles and contrast experiment of BA (C) and *p*-phenyl benzaldehyde (D) with ECA between KZ-8.2-650-D, KZ-8.2-650-S and KZ-8.2-650-R (as reference materials).

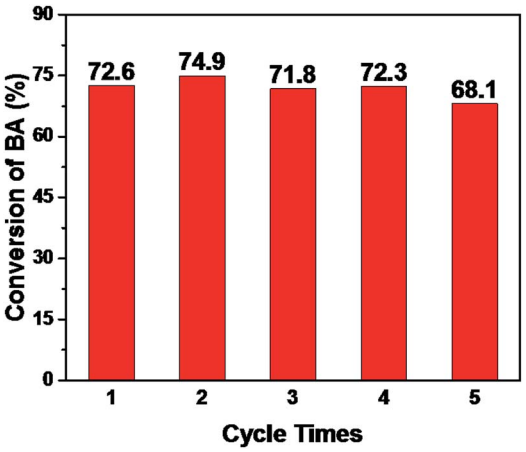

Fig. 8 Recycle experiments of KZ-8.2-650-D.

structures showed 44% conversion of BA with excessive ECA in 30 minutes while nonporous KZ-8.2-650-S just converted 24% of BA, about half conversion of the former. KZ-8.2-650-R got a conversion of 21%, even slightly fewer than that of KZ-8.2-650-S. A more prominent difference was shown for condensation of BA with *p*-phenyl benzaldehyde, which has a much larger molecular size and the reaction rates were inclined to be kinetically controlled by mass transfer efficiency on the basis of KZs' pore structures. For KZ-8.2-650-D with superior surface areas, the conversion of *p*-phenyl benzaldehyde achieved 79.0% within 30 minutes while KZ-8.2-650-S just converted 26.5% of *p*-phenyl benzaldehyde with limited porosity (only 23% for KZ-8.2-650-R). Due to previous report, higher degree of exposure with catalytic sites on larger surface can facilitate diffusion of reactants and products, so as to enhance catalytic performance with more accessible catalytic centers.[30,31] Furthermore, substrates with larger molecular sizes are more likely to be influenced by KZs' pore structures due to critical role of mass transfer during catalytic reactions. The catalyst's stability is tested with recycling experiments and KZ-8.2-650-D maintains its original reactivity for five cascade running cycles with just slightly reducing in BA's conversion (Fig. 8). The same stability is also observed in porosity of KZ-8.2-650-D (Fig. S7†). Mesoporous KZ's performance is among the best recycling ability for alkali metal doped metal oxides as solid bases.[32]

Conclusions

In this report, mesoporous KZ are prepared with a two-step heat treatment from KNO_3 loaded UiO-66. To the best of our knowledge, this is the first time to synthesis of metal-oxide typed solid base with MOFs as precursors. KNO_3@UiO-66 is firstly converted into carbon hybrid KZ, and carbon is converted from organic part of UiO-66. This self-made carbon matrix can act as the mesoporous templates, as well as strengthen the frameworks of mesoporous KZ with high base-resistance ability. With enhanced surface areas and easier accessible basic centers, mesoporous KZ shows accelerated reaction rates over their nonporous counterparts which is synthesized by single-

step calcination. The obtained mesoporous KZ also showed superior catalytic performance, when compared with KZ prepared from the traditional zirconium hydroxides as precursors. In brief, the self-templated cascade transformation opens a new rout to synthesis corrosive and structure-unstable metal oxides from MOFs.

Conflicts of interest

There are no conflicts to declare.

Acknowledgements

Financial support from the National Natural Science Foundation of China (Grant No. 21503024) and the Jiangsu Province Science Foundation for Youth (Grant No. BK20150264, BK20150261) is greatly appreciated. The Priority Academic Program Development of Jiangsu Higher Education Institutions (PAPD) and Jiangsu Key Laboratory of Advanced Catalytic Materials and Technology (Grant No. BM2012110) are also appreciated.

Notes and references

1 H. Hattori, *Chem. Rev.*, 1995, **95**, 537–558.
2 J. Liu, Q. Yang, L. Zhang, H. Yang, J. Gao and C. Li, *Chem. Mater.*, 2008, **20**, 670–677.
3 P. Wang, H. Li, Q. Gao, P.-Z. Li, X. Yao, L. Bai, K. T. Nguyen, R.-Q. Zou and Y. Zhao, *J. Mater. Chem. A*, 2014, **2**, 18731–18735.
4 G. Busca, *Chem. Rev.*, 2010, **110**, 2217–2249.
5 L. Zhu, X.-Q. Liu, H.-L. Jiang and L.-B. Sun, *Chem. Rev.*, 2017, **117**, 8129–8176.
6 L.-B. Sun, X.-Q. Liu and H.-C. Zhou, *Chem. Soc. Rev.*, 2015, **44**, 5092–5147.
7 Y. Wang, W. Y. Huang, Y. Chun, J. R. Xia and J. H. Zhu, *Chem. Mater.*, 2001, **13**, 670–677.
8 H. Duan, Y. Yamada, S. Kubo and S. Sato, *Appl. Catal., A*, 2017, **530**, 66–74.
9 S. Liu, X. Zhang, J. Li, N. Zhao, W. Wei and Y. Sun, *Catal. Commun.*, 2008, **9**, 1527–1532.
10 L. Gong, L.-B. Sun, Y.-H. Sun, T.-T. Li and X.-Q. Liu, *J. Phys. Chem. C*, 2011, **115**, 11633–11640.
11 W. Xia, A. Mahmood, R. Zou and Q. Xu, *Energy Environ. Sci.*, 2015, **8**, 1837–1866.
12 R. R. Salunkhe, Y. V. Kaneti, J. Kim, J. H. Kim and Y. Yamauchi, *Acc. Chem. Res.*, 2016, **49**, 2796–2806.
13 P. Wang, J. Zhao, X. Li, Y. Yang, Q. Yang and C. Li, *Chem. Commun.*, 2013, **49**, 3330–3332.
14 J. Juan-Alcaniz, J. Gascon and F. Kapteijn, *J. Mater. Chem.*, 2012, **22**, 10102–10118.
15 P. Wang, J. Feng, Y. Zhao, S. Wang and J. Liu, *ACS Appl. Mater. Interfaces*, 2016, **8**, 23755–23762.
16 J. H. Cavka, S. Jakobsen, U. Olsbye, N. Guillou, C. Lamberti, S. Bordiga and K. P. Lillerud, *J. Am. Chem. Soc.*, 2008, **130**, 13850–13851.
17 L. Oar-Arteta, T. Wezendonk, X. Sun, F. Kapteijn and J. Gascon, *Mater. Chem. Front.*, 2017, **1**, 1709–1745.
18 K. Shen, X. Chen, J. Chen and Y. Li, *ACS Catal.*, 2016, **6**, 5887–5903.
19 X. Xu, R. Cao, S. Jeong and J. Cho, *Nano Lett.*, 2012, **12**, 4988–4991.
20 Y. Boyjoo, Y. Cheng, H. Zhong, H. Tian, J. Pan, V. K. Pareek, S. P. Jiang, J.-F. Lamonier, M. Jaroniec and J. Liu, *Carbon*, 2017, **116**, 490–499.
21 J. Gao, X. Zhang, S. Xu, F. Tan, X. Li, Y. Zhang, Z. Qu, X. Quan and J. Liu, *Chem.–Eur. J.*, 2014, **20**, 1957–1963.
22 H.-J. Cui, J.-W. Shi, B. Yuan and M.-L. Fu, *J. Mater. Chem. A*, 2013, **1**, 5902–5907.
23 X.-Y. Liu, L.-B. Sun, F. Lu, T.-T. Li and X.-Q. Liu, *J. Mater. Chem. A*, 2013, **1**, 1623–1631.
24 J. Liu, S. Bai, Q. Jin, H. Zhong, C. Li and Q. Yang, *Langmuir*, 2012, **28**, 9788–9796.
25 Y. Wang, W. Y. Huang, Z. Wu, Y. Chun and J. H. Zhu, *Mater. Lett.*, 2000, **46**, 198–204.
26 L. Zhu, F. Lu, X.-D. Liu, X.-Q. Liu and L.-B. Sun, *Chem. Commun.*, 2015, **51**, 10058–10061.
27 L. B. Sun, Y. Chun, F. N. Gu, M. B. Yue, Q. Yu, Y. Wang and J. H. Zhu, *Mater. Lett.*, 2007, **61**, 2130–2134.
28 J. Weitkamp, M. Hunger and U. Rymsa, *Microporous Mesoporous Mater.*, 2001, **48**, 255–270.
29 M. J. Climent, A. Corma, V. Fornés, A. Frau, R. Guil-López, S. Iborra and J. Primo, *J. Catal.*, 1996, **163**, 392–398.
30 P. Wang, S. Bai, J. Zhao, P. Su, Q. Yang and C. Li, *ChemSusChem*, 2012, **5**, 2390–2396.
31 P. Wang, S.-Y. Bai, B. Li and Q.-H. Yang, *Chin. J. Catal.*, 2012, **33**, 1689–1695.
32 J. Zhao, J. Xie, C.-T. Au and S.-F. Yin, *Appl. Catal., A*, 2013, **467**, 33–37.

